Topological Mapping of the Asymmetric Drug Binding to the HERG Potassium Channel By Use of Tandem Dimers

Toshihiko Myokai, Sunghi Ryu, Hirofumi Shimizu & Shigetoshi Oiki

TM, HS, SO: Department of Molecular Physiology and Biophysics, Faculty of Medical Sciences, University of Fukui, Fukui 910-1193, Japan,

SR: Pharmaceutical Research Division, Takeda Pharmaceutical Company Limited, Osaka 532-8686, Japan

Molecular Pharmacology Fast Forward. Published on March 7, 2008 as DOI: 10.1124/mol.107.042085
This article has not been copyedited and formatted. The final version may differ from this version.

Running title: Topological mapping of drug binding to the HERG channel

Corresponding author: Shigetoshi Oiki
Department of Molecular Physiology and Biophysics, Faculty of Medical Sciences, University of Fukui, 23-3 Matsuokashimoaizuki, Eiheiji-cho, Yoshida-gun, Fukui 910-1193, Japan
Phone: 81-776-61-8306
FAX: 81-776-61-8101
e-mail: oiki-fki@umin.ac.jp

The number of text pages: 43 pages
The number of tables: 3 tables
The number of figures: 9 figures
The number of references: 31 references
The number of words in the Abstract: 246 words
The number of words in the Introduction: 301 words
The number of words in the Discussion: 1779 words

The abbreviations used are: HERG: human *ether-à-go-go* related gene product; $V_{1/2}$: the half activation voltage. K_i: the blocking inhibition constant.

Molecular Pharmacology Fast Forward. Published on March 7, 2008 as DOI: 10.1124/mol.107.042085
This article has not been copyedited and formatted. The final version may differ from this version.

Abstract

The human *ether-à-go-go* related gene product (HERG) channel is essential for electrical activity of heart cells and block of this channel by many drugs leads to lethal arrhythmias. Y_{652} and F_{656} of the sixth transmembrane helix are candidates for the drug binding site. In the tetrameric HERG channel a drug with asymmetric structure should interact unevenly with multiple residues from different subunits. To elucidate the topology of the drug-binding site, we constructed tandem dimers of HERG channels and the aromatic Y_{652} and F_{656} residues were replaced by alanine singly or doubly. Eight types of HERG channels, including homo-tetrameric mutants, having different numbers and arrangements of aromatic residues at the blocking site, were studied. Effects of cisapride on channels expressed in *Xenopus* oocytes were examined electrophysiologically. The inhibition constants (K_i) were increased significantly as the diagonal Y_{652}s were deleted, while those for the diagonal F_{656}-deleted mutant were not changed. These results suggest that Y_{652}s from adjacent subunits contributed to the binding. Two types of double mutants of tandem dimers showed significantly distinct affinities, suggesting that the coexistence of Y_{652} and F_{656} on a subunit in diagonal position is crucial to having a high affinity. Thermodynamic double-mutant cycle analyses revealed interactions between Y_{652} and F_{656} upon binding. The kinetics and voltage-dependence of blocking suggested transitions of the binding site from low- to high-affinity. These approaches using a set of mutant HERG channels gave a dynamic picture of the spatial arrangements of residues which contribute to the drug-channel interaction.

Molecular Pharmacology Fast Forward. Published on March 7, 2008 as DOI: 10.1124/mol.107.042085
This article has not been copyedited and formatted. The final version may differ from this version.

Introduction

Malfunction of the human *ether-à-go-go* related gene product (HERG) potassium channels by either hereditary disorders or drug block leads to the long QT syndrome which increases the risk of lethal arrhythmias (Ashcroft, 2000; Haverkamp et al., 2000; Sanguinetti and Tristani-Firouzi, 2006). A unique property of the HERG channel is that it is blocked by a variety of drugs (Haverkamp et al., 2000). Understanding the mechanism of the susceptibility to the wide spectra of molecular species is of primary importance in developing drugs without side effects to HERG channels (Mitcheson et al., 2000). Experimental data have accumulated about the residues which contribute to the drug binding, and the most important residues are Y_{652} and F_{656} in the sixth transmembrane helix (Mitcheson et al., 2000, 2005). The HERG channel is composed of four identical subunits which are assembled into a four-fold symmetric structure (Morais-Cabral et al., 1998); however, the blocking drugs are asymmetric in their structure and large enough to span multiple subunits. Thus, aromatic residues (Y_{652} and F_{656}) from different subunits could contribute unequally to the binding during drug-channel interaction. To identify the contributing residues and their positions in a tetrameric channel, a logical and powerful strategy is to reduce the symmetry of the HERG channel from four-fold into two-fold. We constructed, for the first time, a tandem dimer of the HERG channel and introduced aromatic ring-deleting mutations

Molecular Pharmacology Fast Forward. Published on March 7, 2008 as DOI: 10.1124/mol.107.042085
This article has not been copyedited and formatted. The final version may differ from this version.

(F656A and Y652A). Here we focused on a typical HERG channel blocker, cisapride (Mohammad et al., 1997; Walker et al., 1999; Mitcheson et al., 2000), as a probe for the drug binding sites (Mitcheson et al., 2000). In tandem dimers double-mutations generated different positional arrangements of mutated sites in a channel. A set of mutants, including homo-tetrameric mutants, permitted a systematic approach to elucidate the topological map of the cisapride binding in HERG channel.

Molecular Pharmacology Fast Forward. Published on March 7, 2008 as DOI: 10.1124/mol.107.042085
This article has not been copyedited and formatted. The final version may differ from this version.

Materials and Methods

Construction of tandem dimers. The wild type HERG cDNA was cloned at Takeda Pharmaceutical Company Limited, and subcloned into the *Nhe*I and *Eco*RI sites in pCDNA3.1(+) plasmid expression vector (Invitrogen, Carlsbad, CA). Single or double mutations (Y652A and/or F656A) were generated by the overlap extension polymerase chain reaction (PCR) using PLATINUM *Taq* DNA Polymerase High Fidelity (Invitrogen, Carlsbad, CA) and confirmed by sequencing the mutated region and by restriction enzyme analysis. The homo-tetrameric mutant harboring Y652A or F656A was made by introducing the mutated fragment into the HERG channel gene in the pcDNA3.1(+) vector. The HERG tandem dimmers were constructed by linking two monomers that were prepared separately (Christie et al., 1990; Isacoff et al., 1990; Ruppersberg et al., 1990; Liman, 1992). For the N-terminal side monomer, the wild type or mutant (Y652A) HERG channel gene in pcDNA3.1(+) was modified by deleting its stop codon. For the C-terminal side monomer, the HERG channel gene (wild type, harboring single or double mutations) was subcloned downstream of the in-frame *Eco*RI site (note; the original *Nhe*I site in front of the first methionine of the channel gene was modified to a unique *Eco*RI site when subcloned) in the pKF3 vector (Takara Bio, Japan). To generate tandem dimers, the entire channel coding region in the pKF3 vector was digested with *Eco*RI and ligated into the

Molecular Pharmacology Fast Forward. Published on March 7, 2008 as DOI: 10.1124/mol.107.042085
This article has not been copyedited and formatted. The final version may differ from this version.

pcDNA3.1(+) vector harboring the stop codon-deleted channel gene. The two monomers were linked by the nucleotide sequence of GAATTC. For expression in *Xenopus* oocytes, a stretch of 30 polyA (dA:dT) residues was inserted behind the stop codon.

Western blot analysis. HEK293 cells stably expressing HERG channels were homogenized at 4°C in lysis buffer (50 mM Tris-HCl (pH 7.5), 150 mM NaCl, 1 mM EDTA), containing a protease inhibitor mix (Roche Applied Science) and spun at 500 × *g* for 10 min. Pelletes of the membrane fractions were produced from the low-speed supernatants by centrifugation at 150,000 rpm for 30 min. For Western blots, membrane proteins were separated on 7 % SDS-polyacrylamide gels and transferred onto polyvinylidene difluoride membranes. Membranes were probed with polyclonal rabbit anti-HERG antibody (Chemicon, Temecula, CA) and the antibody was detected with an ECL detection kit (Amersham Bioscience).

Electrophysiological recordings. Two-electrode voltage-clamp experiments were performed. Procedures for the isolation of *Xenopus* oocytes, injection of cRNA and electrophysiological experiments are described in detail (Shimizu et al., 2003) and were approved by the Animal Research Committee of University of Fukui. The bath solution contained 4 mM KCl, 96 mM N-methyl-D-glucamine Cl, 1.8mM $CaCl_2$, 1 mM $MgCl_2$, 5 mM HEPES and pH 7.40. Cisapride

Molecular Pharmacology Fast Forward. Published on March 7, 2008 as DOI: 10.1124/mol.107.042085
This article has not been copyedited and formatted. The final version may differ from this version.

(Accurate Chemicals, Westbury, NY) was dissolved into DMSO to make 10 mM stock solutions and kept at –20°C until use. Voltage clamp experiments were performed on the oocytes 2 to 6 days after injection using a Dagan CA1 amplifier (Dagan Corporation, Minneapolis, IL) at 22-24 °C. For the recordings from oocytes expressing the F656A mutant, which has been known as poor expression of channels (Mitcheson et al., 2000; Milnes et al., 2003), electrophysiological experiments were performed within three days after the injection until the oocyte became damaged. The oocytes were perfused continually with the perfusates at the rate of 1 mL/min using an infusion pump (TE-331, TERMO, Japan). Oocytes exhibiting endogenous currents were excluded from analyses.

Activation and inactivation gate. To characterize the activation gate for mutant channels, the peak amplitudes for the tail currents at -50 mV were plotted as a function of the preceding activation voltages. This tail *I-V* curve was fitted with the Boltzmann function.

$$I_{tail} = \frac{A_1 - A_2}{1 + Exp[(V - V_{1/2})/dx]} + A_2 \qquad (1)$$

where V is the membrane potential, $V_{1/2}$ the half activation voltage, dx the slope factor and A_1 and A_2 are the amplitude factors. For the inactivation gate the current amplitudes at the end of the 3 s

Molecular Pharmacology Fast Forward. Published on March 7, 2008 as DOI: 10.1124/mol.107.042085
This article has not been copyedited and formatted. The final version may differ from this version.

depolarization pulses (isochronal *I-V* curves) were drawn, which were superimposed on the tail *I-V* curves for each channel species (Fig. S1). The isochronal *I-V* curves show a typical bell shape, indicating the characteristic inactivation of HERG channel. The double-Boltzmann function was used for the fitting.

$$y = \frac{A_2}{1 + Exp[(V - V_{1/2}) / dx] + Exp[(V - V_{inac}) / dx_{inac}]} + A_1 \qquad (2)$$

where V_{inac} and dx_{inac} values were the half inactivation voltage and the slope factor. A_1 and A_2 are the amplitude factors. In this fitting the fitted parameters from the activation data ($V_{1/2}$ and dx,) were used.

Blocking inhibition constants. Block of the HERG currents at each cisapride concentration was evaluated after the steady state was reached. This was performed by eliciting repeatedly 3.5-s depolarization pulses to +20 mV followed by repolarization at –50 mV an interval of 20 s (the holding potential was –80 mV) and checking the current amplitudes reached at the steady state. At low concentrations it took several tens of minutes. Inhibition constants (K_i) were obtained from the peak amplitudes of the tail currents at –50 mV preceded by the depolarizing pulse to +20 mV for 3 s. From concentration dependence of current amplitude K_i values and the Hill

Molecular Pharmacology Fast Forward. Published on March 7, 2008 as DOI: 10.1124/mol.107.042085
This article has not been copyedited and formatted. The final version may differ from this version.

coefficients (*n*) were obtained from the concentration dependence of current amplitude by fits to the equation:

$$I / I_0 = \frac{1}{1 + ([cisapride] / K_i)^n} \quad (3)$$

Voltage-dependence of the binding affinity was obtained by fitting the K_i values with the function:

$$K_i = K_0 \, \mathrm{Exp}[-e \, z \, V / kT] \quad (4)$$

where K_0 represents the inhibition constant at 0 mV, *z* is the gating charge and *e*, *k* and *T* have the usual meanings.

Thermodynamic double-mutant cycle. To estimate the interaction free energy upon binding, thermodynamic double-mutant cycle analysis was applied (Schreiber and Fersht, 1995; Ranganathan et al., 1996; Fersht, 1999; Yan et al., 2006). First, the binding free energy (*G*) was evaluated from the inhibition constant:

Molecular Pharmacology Fast Forward. Published on March 7, 2008 as DOI: 10.1124/mol.107.042085
This article has not been copyedited and formatted. The final version may differ from this version.

$$G = kT \log K_i \quad (5)$$

The differences in the affinities between two channel species were obtained from the differences in G. For example, the change in the binding free energy by a single mutation relative to the wild type ($\Delta G_{singleM\text{-}WT}$) is:

$$\Delta G_{singleM\text{-}WT} = G_{singleM} - G_{WT} \quad (6)$$

A double mutant can be regarded as a combination of two single mutations. Therefore, ΔG for the double mutant compared to WT is:

$$\Delta G_{doubleM\text{-}WT} = \Delta G_{singleM\text{-}WT} + \Delta G_{doubleM\text{-}singleM} \quad (7)$$

The ΔG for mutation of F_{656} site introduced into either WT or Y652A is $\Delta G_{singleM-WT}$ or $\Delta G_{doubleM-singleM}$. The difference in these energies defines the coupling energy, $\Delta\Delta G_{int}$, which represents interaction between two sites:

$$\Delta\Delta G_{int} = \Delta G_{singleM-WT} - \Delta G_{doubleM-singleM} \quad (8)$$

Molecular Pharmacology Fast Forward. Published on March 7, 2008 as DOI: 10.1124/mol.107.042085
This article has not been copyedited and formatted. The final version may differ from this version.

The values of $\Delta\Delta G_{int}$ indicate cooperativity between residues.

Blocking kinetics. The concentration dependence of the apparent blocking rate (= the reciprocal of the time constant) for a simple three-state model can be expressed as the following equation, if the binding and unbinding kinetics are fast relative to the subsequent transition represented by the rate constants of k_3 and k_{off}:

$$blocking\_rate = \frac{[B]k_3}{[B] + K_f} + k_{off} \quad (9)$$

K_f (= k_2/k_1) is the dissociation constant for the initial binding site (see Supplemental data).

Data analysis. Experimental data were analyzed with Origin software (OriginLab corporation, Northampton, MA) and Mathematica (Wolfram Research Inc., Champaign, IL). Data are presented as mean ± S.E.M.

Molecular Pharmacology Fast Forward. Published on March 7, 2008 as DOI: 10.1124/mol.107.042085
This article has not been copyedited and formatted. The final version may differ from this version.

Results

Expression of tandem dimers.

We constructed seven mutants (Table 1), which were expressed in *Xenopus* oocytes and HEK 293 cells (Ando et al., 2005). Western blot was performed on HEK 293 cells to verify the expression of the mutants (Figure 1B). Tandem dimers showed protein bands at the expected locations. For monomeric channels double protein bands were observed at around 135/155 kDa, as has been reported for monomeric HERG channels (Zhou et al., 1998; Ficker et al., 2004). For tandem dimers double bands were seen at 270/310 kDa.

Electrophysiological characterization of mutant channels.

The electrophysiological properties of mutant and wild type (WT) HERG channels expressed in *Xenopus* oocytes were examined. Gating properties for WT and all the mutants, including the tandem WT (td[wt : wt]), were measured from the current traces elicited by depolarizing pulses (Figure 2A). The activation gating and inactivation gating were measured by plotting the tail *I-V* curves and the isochronal *I-V* curves at the end of the depolarization pulses (Fig. 2A inset and Fig. S1 in Supplemental data). The voltage dependence of activation and inactivation gating for WT and td[wt : wt] were basically similar, suggesting that concatenation did not affect the

Molecular Pharmacology Fast Forward. Published on March 7, 2008 as DOI: 10.1124/mol.107.042085
This article has not been copyedited and formatted. The final version may differ from this version.

steady-state gating. In all the mutants the activation curves were shifted slightly in the negative direction (Table 2), although the slope factor was not changed significantly. Deactivation for td[wt : wt] was faster compared to the WT. This tendency seemed to hold for all the tandem dimers. In the tandem dimers a linker between subunits was short, which may accelerate the deactivation rate. In fact, a contribution of the N-terminal domain to the deactivation gating of HERG channel has been reported (Morais-Cabral et al., 1998; Wang et al., 2000). Then a cytoplasmic domain between subunits in the tandem dimers might be restricted by the short linker.

The steady-state blocking of cisapride.

To examine the concentration dependence of current blocking to cisapride, it was perfused continually throughout the experiment and HERG currents were evaluated after the block reached the steady-level. The current traces showed (Figure 2B) a slow decay during depolarizing pulses for WT and some of the other mutants and mostly reached the steady state at the end of the depolarization pulses. This decay was not observed for Y652A, F656A and td[Y652A : F656A]. K_i values were obtained from the concentration dependence of the peak amplitudes of the tail currents at –50 mV (Table 3). The Hill coefficients were nearly one, suggesting the binding stoichiometry of the drug-HERG channel as one to one.

Molecular Pharmacology Fast Forward. Published on March 7, 2008 as DOI: 10.1124/mol.107.042085
This article has not been copyedited and formatted. The final version may differ from this version.

The free energy of the binding of cisapride to HERG channels, which was calculated from the K_i values as $G = kT \log K_i$, is shown in Figure 3. It is clearly seen that not only the number of the aromatic residues but also the spatial location of each residue is crucial for the binding affinity. The affinities were reduced dramatically by complete deletion of either of the aromatic residues (F656A and Y652A), confirming the previous reports (Mitcheson et al., 2000). The levels of the binding energy for WT and td[wt : wt] were similar, indicating that the concatenation did not affect the binding of the blocker. The affinity for td[wt : F656A] was similar to that of WT, which indicates that, although F_{656} contributed to the binding significantly, at most two F_{656}s from diagonal subunits were required for binding. On the other hand, the affinity of td[wt : Y652A] was significantly reduced, suggesting that Y_{652} residues from adjacent subunits contributed to the binding. This is the first experimental observation that cisapride may interact with multiple Y_{652}s.

The sequence of the binding energies among mutants with the same number of aromatic residues was most informative (see the rightmost column of Figure 3). First, to have both F_{656} and Y_{652} aromatic residues on a channel is more important for high affinity binding than to have single-species aromatic rings. Secondly, the four fold higher affinity (the difference of the binding free energy: ΔG = 3.5 kJ/mol) of td[wt : Y652AF656A] than td[Y652A : F656A] indicates that having both Y_{652} and F_{656} on a same subunit is crucial for a channel to show a high affinity. Energetic considerations provided further clues on the contributions of residues to the

Molecular Pharmacology Fast Forward. Published on March 7, 2008 as DOI: 10.1124/mol.107.042085
This article has not been copyedited and formatted. The final version may differ from this version.

binding and interactions between residues upon binding, which will be discussed below.

Voltage-dependent blocking.

Voltage dependent blocking was evaluated from current traces elicited by depolarizing pulses (Figure 2B). In WT and some mutants, the slow decay of the currents seen at depolarized potentials was accelerated as the membrane potential was depolarized more. In the presence of cisapride, the tail *I-V* curves (the peak amplitudes of the tail currents as a function of the preceding depolarizing voltages) showed a maximum at around 0 mV for WT (Figure 4A). The current amplitudes were depressed slightly as the membrane potential was depolarized further. This pattern is an indication of the presence of voltage-dependent block (Walker et al., 1999; Sanchez-Chapula et al., 2003). At each voltage the K_i values were calculated from the concentration-dependence curves (Figure 4B).

Similarly, the K_i values for mutants at different membrane potentials were obtained (see Supplemental data) and are also shown in Figure 4B. K_i values were voltage-dependent for WT, td[wt : wt], td[wt : F656A], td[wt : Y652AF656A] and F656A. td[Y652A : F656A], td[wt : Y652A] and Y652A did not show voltage dependence. It should be noted that voltage-dependence was almost abolished even when only two diagonal Y_{652}s, not four of them, were deleted.

Molecular Pharmacology Fast Forward. Published on March 7, 2008 as DOI: 10.1124/mol.107.042085
This article has not been copyedited and formatted. The final version may differ from this version.

Kinetics of blocking.

The currents of some of the mutants as well as WT exhibited slow decays at depolarized potentials while others did not. To examine the mechanisms underlying the different blocking kinetics, we focused on F656A. F656A showed voltage-dependent block but the currents did not show a decay at depolarized potentials. The shapes of the tail currents were changed in the presence of cisapride (Figure 5). Expansion of the tail current traces showed that the currents reached their peak with a slower rising phase in the presence of cisapride (the right panel), which was not observed in the absence of cisapride (the left panel). The slowly rising phases became more prominent as the preceding voltages were more depolarized. The tail-currents of F656A were fitted with a double-exponential function in the absence of cisapride (the recovery from the inactivation and de-activation components) and with a triple-exponential function in the presence of cisapride. The novel kinetic component having an intermediate time constant (~100 ms) between those of recovery from the inactivation and de-activation (see Supplemental data) seems to be related to blocking. In fact the time constant of the intermediate component was reduced as the cisapride concentration was increased. This is in contrast to the time constant for recovery from the inactivation being unaltered. These results suggest that the intermediate component represented unblocking kinetics. The amplitudes of the unblocking component increased as the

Molecular Pharmacology Fast Forward. Published on March 7, 2008 as DOI: 10.1124/mol.107.042085
This article has not been copyedited and formatted. The final version may differ from this version.

pre-potential was more depolarized (see Supplemental data). This is because more channels had been blocked at more depolarized potentials and those blocked channels released more drug upon repolarization. These are typical voltage-dependent unblocking kinetics (Hille, 2001). The plot of the apparent rate of block (= the reciprocal of the unblocking time constant) as a function of cisapride concentration showed a nearly linear relationship (Figure 7A, open diamonds). This kinetic feature will be discussed with respect to the blocking mechanism below.

For other types of channels, the kinetics of tail current were examined but kinetic components relevant to the unblocking of cisapride were not found. However, the blocking kinetics was evaluated on a longer time scale from a pulse protocol shown in Figure 6. Depolarizing pulses to +20 mV were prolonged progressively from 50 ms to 7000 ms and the tail currents at –50 mV were recorded. The peaks of the tail currents were plotted as a function of the duration of the depolarization (the envelope current; Fig. 6B inset). In the absence of cisapride, the current envelopes reached saturation as the depolarization pulses were prolonged (filled square symbols in the inset). These represent the time courses of the activation gating. In the presence of cisapride the envelope currents were depressed as the duration of depolarization was prolonged. This depression was seen for WT, td[wt : wt], td[wt : F656A], td[wt : Y652A] and td[wt : Y652AF656A] (these channels are named here as the high affinity channels) but not for td[Y652A : F656A], F656A and Y652A. The envelope currents were fitted with a

double-exponential function (Figure 6B inset). The fast and slow components represent the time course of activation and block. The envelope experiments were performed at different cisapride concentrations. The time constants for activation for all the channel species were similar and did not change significantly with cisapride concentration. On the other hand, the time constants for the blocking changed significantly. For channel species exhibiting depression of the current envelopes, plots of the apparent rates of block (= reciprocal of the blocking time constants) as a function of cisapride concentration showed nearly linear relationships (Figure 7A).

Molecular Pharmacology Fast Forward. Published on March 7, 2008 as DOI: 10.1124/mol.107.042085
This article has not been copyedited and formatted. The final version may differ from this version.

Discussion

In this study tandem dimers of HERG channels were constructed for the first time to investigate the mechanisms underlying the block of HERG channels. Introducing single or double mutations into tandem dimers, including single-mutation homotetramers, produced channels with variable arrangements of aromatic residues. The tandem dimers exhibited channel activity with the fast deactivation. This might be a signature that both subunits of the concatenated dimers were incorporated into tetrameric channels, since a cytoplasmic domain between concatenated subunits was restricted, which affected the deactivation gating (Morais-Cabral et al., 1998; Tu and Deutsch, 1999; Wang et al., 2000). Interactions between cisapride and these mutant HERG channels were examined electrophysiologically and the steady state binding, its voltage dependence and the kinetics of block were analyzed.

Binding energetics and topology

The set of mutants revealed the importance of the spatial arrangement of distinct residues to the binding. In this study we found that cisapride binding was not confined to a single subunit but spans multiple subunits in a tetrameric channel: Y_{652}s of adjacent subunits contribute to the binding., In contrast, at most two of F_{656} in diagonal subunits, rather than those in adjacent

Molecular Pharmacology Fast Forward. Published on March 7, 2008 as DOI: 10.1124/mol.107.042085
This article has not been copyedited and formatted. The final version may differ from this version.

subunits, were enough for binding, although complete loss of F_{656} (F656A) destabilized the binding dramatically. For the high affinity binding, retaining intact subunits seems to be important.

For the two double mutants (td[wt : Y652AF656A] and td[Y652A : F656A]), the binding energy differed significantly, which indicates the importance of the arrangements of the aromatic residues in a channel. The contribution of residues to the binding and the interactions between residues upon binding can be evaluated quantitatively by examining the coupling energies ($\Delta\Delta G_{int}$) in the thermodynamic double-mutant cycle analysis (see Methods, Schreiber and Fersht, 1995; Ranganathan et al., 1996; Fersht, 1999; Yan et al., 2006). For each of two double mutants, a cyclic diagram was drawn (Figure 8A). In these diagrams a double mutant can be regarded as the consequences of two successive single mutations reached through two different routes. Inspection of a set of cartoons for a cycle gives ideas how the residues interact upon drug binding.

For the upper cycle (towards td[wt : Y652AF656A]), the cartoons for four channel species exhibit a common feature, i.e., a diagonal pair of subunits is intact. This means that the double mutant was generated by introducing two mutations successively into subunits adjacent to the intact subunits. From a thermodynamic relationship (Eq. 8), $\Delta\Delta G_{int}$ of 0.3 kJ/mol was obtained. This value of $\Delta\Delta G_{int}$ did not deviate statistically from zero, indicating that no interaction took place between Y_{652} and F_{656} upon binding. The results indicate that, as far as intact subunits were

Molecular Pharmacology Fast Forward. Published on March 7, 2008 as DOI: 10.1124/mol.107.042085
This article has not been copyedited and formatted. The final version may differ from this version.

retained in a channel, Y_{652} and F_{656} residues on the subunits adjacent to the intact subunits contributed to the binding independently of each other. This additivity is important since it suggests that deleting bulky aromatic rings in two sites did not significantly change the structures of the binding site (Fersht, 1999). This is an implicit assumption for studies of mutational analysis in general but has not been supported for HERG channels until this study.

Next, look at another cycle with td[Y652A : F656A] as a double mutant (Figure 8A lower panel). The $\Delta\Delta G_{int}$ value of –3.1 kJ/mol indicates significant interactions. The negative sign of $\Delta\Delta G_{int}$ represents that F_{656} and Y_{652} contribute to the binding with negative interactions. What is the origin of this cooperativity? In the double-mutant cycle analysis, significant coupling is explained as being attributable to the proximity of mutated residues (Schreiber and Fersht, 1995). The set of cartoons demonstrates that two mutational sites are proximally-positioned on the two adjacent subunits. Then the strong interaction can be interpreted that F_{656} and Y_{652} residues on two adjacent subunits are closely apposed.

In the thermodynamic double-mutant cycle analysis, two different types of interactions were elucidated. Y_{652} and F_{656} on the same subunits interact additively (upper cycle) and Y_{652} and F_{656} on adjacent subunits interact cooperatively (lower cycle). One may imagine that the Y_{652} and F_{656} residues from adjacent subunits are placed closer than those placed on the same subunits.

Molecular Pharmacology Fast Forward. Published on March 7, 2008 as DOI: 10.1124/mol.107.042085
This article has not been copyedited and formatted. The final version may differ from this version.

Hypothetical binding pose of cisapride in the high-affinity site of HERG channels

Cisapride contains two aromatic moieties and one basic tertiary nitrogen (Figure 8A) that can interact with the aromatic amino acids by cation-π and π-π interactions or by hydrophobic interactions (Mitcheson et al., 2000; Fernandez et al., 2004). Here we propose a possible binding mode of cisapride. Two Y_{652}s from adjacent subunits and one F_{656} form a favorable binding site, while F_{656} in the adjacent subunit hinders the binding (Figure 8B).

This mode of interaction was compared with the computational docking model built on a homology model of HERG channel (Aronov and Goldman, 2004; Österberg and Åqvist, 2005; Farid et al., 2006). It was predicted that multiple simultaneous aromatic ring stacking and/or hydrophobic interactions between Y_{652} and F_{656} side chains and aromatic/hydrophobic blocker groups are involved in the docking poses (Farid et al., 2006). It was also predicted that Y_{652} and F_{656} from multiple subunits might be involved in cisapride binding (Farid et al., 2006). This docking pose is in general agreement with our experimental data.

Voltage-dependent block suggests a sequential binding mechanism.

The voltage-dependence of cisapride block has been reported (Walker et al, 1999) and in this study the K_i values for WT and some mutants were voltage-dependent (Figure 4). Not only Y652A, but also td[Y652A : F656A] and td[wt : Y652A] exhibited voltage-independence. The

Molecular Pharmacology Fast Forward. Published on March 7, 2008 as DOI: 10.1124/mol.107.042085
This article has not been copyedited and formatted. The final version may differ from this version.

presence or absence of the voltage-dependence for different mutants indicates that voltage-dependent block occurs through voltage-dependent conformational changes of the binding site rather than the binding of a charged drug to the site under the influence of the membrane electric field. To introduce voltage-dependence into the blocking mechanism, a sequential binding model was applied:

$$O \overset{[B]}{\leftrightarrow} B_1 \leftrightarrow B_2$$

in which O represents the open state, B_1 the first blocked state and B_2 is the subsequent blocked state. [B] indicates the concentration of blocker. In this model drug-bound channels undergo conformational changes between the B_1 and B_2 states in a voltage-dependent manner, leading to more stable binding of the drug in the B_2 state. A similar model has been proposed for blocking by chloroquine (Sanchez-Chapula et al., 2002).

The behavior of channels exhibiting voltage-independent blocking (Y652A, td[wt : Y652A] and td[Y652A : F656A]) can be explained by the absence of transitions from B_1 to B_2. In these mutants some of Y_{652}s were deleted, suggesting that the Y_{652} residues contribute to the voltage-dependence through changes in their orientation upon depolarization (Sanchez-Chapula et al., 2003). In this study we found that the voltage-dependence was almost abolished even for

Molecular Pharmacology Fast Forward. Published on March 7, 2008 as DOI: 10.1124/mol.107.042085
This article has not been copyedited and formatted. The final version may differ from this version.

td[wt : Y652A]. On the other hand, td[wt : Y652AF656A] retained voltage-dependence. It is suggested that rearrangements of Y_{652}s seem to be affected by surrounding F_{656}s.

Kinetic data suggest a low affinity binding site.

Blocking kinetics were evaluated by two different methods: Unblocking kinetics after repolarization and slow blocking kinetics by the envelope analyses. In either case the apparent rate constants of block were found to be a nearly linear function of the cisapride concentrations (Figure 7A). If the blocking kinetics is described by a simple two state model, the rate constant of block should be linear. Sub-linearity of the blocking rate constant can be accounted for by the presence of an intermediate state of block. Therefore at least three states are necessary to describe the kinetic data (Fercht, 1999). This corresponds to the linear 3-state model proposed for the voltage-dependent block. Sub-linearity of the kinetic data demands that the model has a fast low-affinity binding process followed by a slow transition:

$$O \underset{k_2}{\overset{[B]k_1}{\Leftrightarrow}} B_1 \underset{k_4}{\overset{k_3}{\leftrightarrow}} B_2$$

where k_1 through k_4 represent the rate constants and the white arrow indicates fast transitions.

The equation 9 (see Methods and Supplemental data) for the apparent blocking rate was used

Molecular Pharmacology Fast Forward. Published on March 7, 2008 as DOI: 10.1124/mol.107.042085
This article has not been copyedited and formatted. The final version may differ from this version.

to fit the data and values of K_f (the dissociation constant for the initial binding site), k_3 and k_{off} (= k_4) were obtained (Figure 7B, also see Supplemental data). For the high affinity channels (WT, td[wt : wt], td[wt : F656A], td[wt : Y652A] and td[wt : Y652AF656A]), the k_{off} values were very slow (< 0.32/s; Figure 7A legend). This slow unblocking accounts for the apparent absence of the unblocking at the time of peak for tail current measurements: the high affinity blocked state (B_2) did not return to the open state through B_1 during the early course of the tail currents. K_i values evaluated from the tail currents, thus, reflect blocking at depolarized potentials. k_3 was so slow that the high affinity binding site scarcely appeared during short depolarizing pulses. Slow appearance of the high affinity site and slow release from it lead to slow accumulation of blocking during repeated depolarizations.

The relationships between the inactivated state and the high affinity binding state have been discussed. The inactivation state is a state for a non-conducting selectivity filter, while the high affinity binding state represents arrangements of aromatic residues in the central cavity. Spacially, they are closely located. However, the kinetic analyses suggest that the high affinity site appears later (Fig. 7A legends) than the fast inactivation. Then it is likely that the inactivation may induce the transition to the high affinity state. This is in agreement to the previous papers that inactivation controlled the high-affinity binding (Numaguchi et al., 2000).

For F656A the K_f and k_{off} (Figure 7B and 7C legend) values were significantly greater, which

Molecular Pharmacology Fast Forward. Published on March 7, 2008 as DOI: 10.1124/mol.107.042085
This article has not been copyedited and formatted. The final version may differ from this version.

led to the low affinity of this mutant. Voltage-dependence of this channel indicates that the transition between B_1 and B_2 was retained. Then, the absence of current decay in the envelope experiment is related to the fast transition from the B_1 to the B_2 state. This feature suggests that F_{656}s may retard the rearrangements of Y_{652}s.

An overview of the kinetic features of channel species revealed that only in F656A the initial binding site show a reduced affinity and the other channels did not. All of the latter possess at least two diagonal F_{656}s in common. Therefore, it is suggested that the diagonal F_{656}s may form the initial binding site for cisapride.

Conclusion.

Combining the steady-state block data, its voltage-dependence and the kinetic data suggests the hypothetical binding process shown in Figure 9. Cisapride binds to the low affinity site constituted by diagonal F_{656}s. Meanwhile, voltage-dependent conformational changes reorient the Y_{652}s with F_{656} and form the high affinity site produced by two adjacent Y_{652}s and F_{656} but hindered by adjacent F_{656}.

In this study a topological picture of the interaction between HERG and cisapride was obtained. Systematic approaches using a set of mutants and thermodynamic and kinetic analyses mapped the binding site and the blocking process. This approach will be applied to understand

Molecular Pharmacology Fast Forward. Published on March 7, 2008 as DOI: 10.1124/mol.107.042085
This article has not been copyedited and formatted. The final version may differ from this version.

better the mechanism of action between HERG channels and the broad spectrum of blocking substances.

References

Ando H, Kuno M, Shimizu H, Muramatsu I and Oiki S (2005) Coupled K^+-water flux through the HERG potassium channel measured by an osmotic pulse method. *J. Gen. Physiol* **126**:529-538.

Aronov AM and Goldman BB (2004) A model for identifying HERG K^+ channel blockers. *Bioorg Med Chem* **12**:2307-2315.

Ashcroft FM (2000) *Ion Channels and Disease: Channelopathies.* Academic Press, London.

Christie MJ, North RA, Osborne PB, Douglass J and Adelman JP (1990) Heteropolymeric potassium channels expressed in *Xenopus* oocytes from cloned subunits. *Neuron* **4**:405–411.

Farid R, Day T, Friesner RA and Pearlstein RA (2006) New insights about HERG blockade obtained from protein modeling, potential energy mapping, and docking studies. *Bioorg Med Chem* **14**:3160-3173.

Fernandez D, Ghanta A, Kauffman GW and Sanguinetti MC (2004) Physicochemical features of the hERG channel drug binding site. *J Biol Chem* **279**:10120-10127.

Fersht AR (1999) *Structure and Mechanism in Protein Science: A Guide to Enzyme Catalysis and Protein Folding.* Freeman and Company, New York.

Ficker E, Kuryshev YA, Dennis AT, Obejero-Paz C, Wang L, Hawryluk P, Wible BA and Brown AM (2004) Mechanisms of arsenic-induced prolongation of cardiac repolarization. *Mol*

Pharmacol **66**:33–44.

Haverkamp W, Breithardt G, Camm AJ, Janse MJ, Rosen MR, Antzelevitch C, Escande D, Franz M, Malik M, Moss A and Shah R (2000) The potential for QT prolongation and pro-arrhythmia by non-anti-arrhythmic drugs: Clinical and regulatory implications Report on a Policy Conference of the European Society of Cardiology. *Cardiovasc Res* **47**:219–233.

Hille B (2001) *Ion Channels of Excitable Membranes*, 3rd Ed. Sinauer Associates Inc, Sunderland.

Isacoff EY, Jan YN and Jan LY (1990) Evidence for the formation of heteromultimeric potassium channels in *Xenopus* oocytes. *Nature* **345**:530-534.

Liman E, Tytgat J and Hess P (1992) Subunit stoichiometry of a mammalian K^+ channel determined by construction of multimeric cDNAs. *Neuron* **9**: 861-871.

Milnes JT, Crociani O, Arcangeli A, Hancox JC and Witchel HJ (2003) Blockade of HERG potassium currents by fluvoxamine: incomplete attenuation by S6 mutations at F656 or Y652. *Br J Pharmacol* **139**:887-898.

Mitcheson JS, Chen J, Lin M, Culberson C and Sanguinetti MC (2000) A structural basis for drug-induced long QT syndrome. *Proc Natl Acad Sci USA* **97**:12329-12333.

Mitcheson J, Perry M, Stansfeld P, Sanguinetti MC, Witchel H and Hancox J (2005) Structural determinants for high-affinity block of hERG potassium channels. *Novartis Found Symp*

266:136-150.

Mohammad S, Zhou Z, Gong Q and January CT (1997) Blockage of the HERG human cardiac K^+ channel by the gastrointestinal prokinetic agent cisapride. *Am J Physiol* **273**:H2534-H2538.

Morais-Cabral JH, Lee A, Cohen SL, Chait BT, Li M and Mackinnon R (1998) Crystal structure and functional analysis of the HERG potassium channel N terminus: a eukaryotic PAS domain. *Cell* **95**:649-655.

Numaguchi H, Mullins FM, Johnson JP Jr, Johns DC, Po SS, Yang IC-H, Tomaselli GF and Balser JR (2000) *Circ Res* **87**:1012-1018.

Österberg F and Åqvist J (2005) Exploring blocker binding to a homology model of the open hERG K^+ channel using docking and molecular dynamics methods. *FEBS Lett* **579**:2939-2944.

Ranganathan R, Lewis JH and MacKinnon R (1996) Spatial localization of the K^+ channel selectivity filter by mutant cycle-based structure analysis. *Neuron* **16**:131-139.

Ruppersberg JP, Schröter KH, Sakmann B, Stocker M, Sewing S and Pongs O (1990) Heteromultimeric channels formed by rat brain potassium-channel proteins. *Nature* **345**:535–537.

Sanchez-Chapula JA, Navarro-Polanco, RA, Culberson C, Chen J and Sanguinetti MC (2002) Molecular determinants of voltage-dependent human *ether-a-go-go* related gene (HERG) K^+ channel block. *J Biol Chem* **277**:23587-23595.

Sanchez-Chapula JA, Ferrer T, Navarro-Polanco RA and Sanguinetti MC (2003) Voltage-dependent profile of human *ether-a-go-go*-related gene channel block is influenced by a single residue in the S6 transmembrane domain. *Mol Pharmacol* **63**:1051–1058.

Sanguinetti MC and Tristani-Firouzi M (2006) hERG potassium channels and cardiac arrhythmia. *Nature* **440:**463-469.

Schreiber G and Fersht AR (1995) Energetics of protein-protein interactions: analysis of the barnase-barstar interface by single mutaitons and double mutant cycles. *J Mol Biol* **248**:478-486.

Shimizu H, Toyoshima C and Oiki S (2003) Interaction between tetraethylammonium and permeant cations at the inactivation gate of the HERG potassium channel. *Jpn J Physiol* **53**:25-34.

Tu L and Deutsch C (1999) Evidence for Dimerization of Dimers in K1 Channel Assembly *Biophys. J.* **76**:2004–2017.

Walker BD, Singleton CB, Bursill JA, Wyse KR, Valenzuela SM, Qiu MR, Breit SN and Campbell TJ (1999) Inhibition of the human ether-a-go-go-related gene (HERG) potassium channel by cisapride: affinity for open and inactivated states. *Br J Pharmacol* **128**:444-450.

Wang J, Myers CD and Robertson GA (2000) Dynamic control of deactivation gating by a soluble amino-terminal domain in HERG K^+ channels. *J Gen Physiol* **115**:749-758.

Yan D, Meyer JK and White MM (2006) Mapping residues in the ligand-binding domain of the 5-HT_3 receptor onto *d*-Tubocurarine structure. *Mol Pharmaco*. **70**:571-578.

Zhou Z, Gong Q, Ye B, Fan Z, Makielski JC, Robertson GA, and January CT (1998) Properties of HERG channels stably expressed in HEK 293 cells studied at physiological temperature. *Biophys J* **74**:230–241

Molecular Pharmacology Fast Forward. Published on March 7, 2008 as DOI: 10.1124/mol.107.042085
This article has not been copyedited and formatted. The final version may differ from this version.

Footnotes

Acknowledgements: This work is supported by Grant-in-Aid for Scientific Research from the Ministry of Education, Science, Sports, and Culture, Japan. We would like to thank R. Horn (Jefferson Medical College), Y. Imai (Takeda Pharmaceutical Company Limited), S. Morishima, M. Iwamoto and C. Edwards for discussion and T. Goto for secretarial assistance.

Molecular Pharmacology Fast Forward. Published on March 7, 2008 as DOI: 10.1124/mol.107.042085
This article has not been copyedited and formatted. The final version may differ from this version.

Legends for figures

Figure 1. Mutants of HERG channels. **(A)** A schematic diagram of the tandem dimer construct of the HERG gene. **(B)** Western blot analyses of homo-tetrameric and tandem-dimeric HERG gene products.

Figure 2. Representative current traces for WT and mutant HERG channels. Currents were elicited by 3-s step pulses from –100 to +40 mV with 10 mV increments followed by 3-s pulses to –50 mV (the holding potential was –80 mV). In this figure the current amplitudes were normalized to emphasize the differences among the various channels. **(A)** Current traces for HERG channels in the absence of cisapride. Cartoons represent the arrangements of Y_{652} and F_{656} residues around the symmetrical axis of the channel. The partial overlap of the symbols for Y_{652} and F_{656} show that they are on the same subunit. Small circles represent mutations to alanine. Schemes with linkers represent tandem dimers. For tandem dimers N- and C-terminal subunits were arranged counter-clockwise. **Inset)** The tail *I-V* curves (open symbols) and the isochronal I-V curves (closed symbols) at the end of the depolarizing pulses for WT (black) and td[wt : wt] (red). **(B)** Current traces in the presence of cisapride. Cisapride concentrations (μmol/L) were 0.63 for WT, 0.25 for td[wt : wt], 0.63 for td[wt : F656A], 0.63 for td[wt : Y652AF656A], 1.6 for

Molecular Pharmacology Fast Forward. Published on March 7, 2008 as DOI: 10.1124/mol.107.042085
This article has not been copyedited and formatted. The final version may differ from this version.

F656A, 0.63 for td[wt : Y652A], 1.6 for td[Y652A : F656A] and 10 for Y652A. **Inset)** The voltage command.

Figure 3. The binding energetics. The vertical axis represents the free energy of binding. The binding energy for each mutant is shown as a level bar. Each column represents channel species having the same numbers of aromatic residues.

Figure 4. Voltage-dependent block. **(A)** The tail *I-V* curves of WT in the absence and in the presence of increased concentrations of cisapride. **(B)** Voltage-dependence of K_i values for WT and mutant HERG channels. The scale of the vertical axis is logarithmic. Symbols indicate: ○: WT, ▼: td[wt : F656A], ●: td[wt : wt], ■: td[wt : Y652AF656A], ▲: td[wt : Y652A], ♦: td[Y652A : F656A], ∇: F656A, Δ: Y652A. Voltage dependence of the block was expressed by the gating charge (see Supplemental data): 0.40 *e* for WT, 0.48 *e* for td[wt : wt], 0.37 *e* for td[wt : F656A], 0.03 *e* for td[wt : Y652A], 0.01 *e* for td[Y652A : F656A], 0.21 *e* for td[wt : Y652AF656A], 0.33 *e* for F656A, and –0.10 *e* for Y652A (*e* is the elementary charge). The value for F656A was corrected for the unblocking (see Supplemental data).

Figure 5. Unblocking of cisapride from F656A. The left panel shows current traces at different

Molecular Pharmacology Fast Forward. Published on March 7, 2008 as DOI: 10.1124/mol.107.042085
This article has not been copyedited and formatted. The final version may differ from this version.

membrane potentials (upper) along with those of tail currents on an expanded time scale in the absence of cisapride (lower). The right panel shows current traces at 1.6 μmol/L cisapride. A slow rising phase appeared in the presence of cisapride. Kinetic analyses were performed on the tail current traces (see detail in Supplemental data).

Figure 6. Envelope analyses of HERG channels without (A) and with cisapride (B). **A.** Representative traces of envelope current for WT and mutants. **Inset)** The command potentials. The longest depolarization pulse was 7 s. **B.** Representative traces of envelope current for WT and mutants at the following cisapride concentrations (μmol/L): 0.25 for WT, 0.25 for td[wt: wt], 0.63 for td[wt: F656A], 0.25 for td[wt: Y652AF656A], 4.0 for F656A, 0.63 for td[wt: Y652A], 1.6 for td[Y652A : F656A], 10.0 for Y652A. It should be noted that current traces early in depolarization pulses for pulses of different durations overlapped completely. This signifies that the currents were recorded in the steady-state of blocking. **Inset)** The time course of block for WT. The peaks of the tail currents were plotted as a function of the duration of depolarizing pulses. The time courses of the currents were fitted with a double-exponential function (curved lines). Current data with a fitted line were shown for different cisapride concentrations. As the cisapride concentrations were increased, current amplitudes were depressed and the decay of current (blocking) was accelerated.

Molecular Pharmacology Fast Forward. Published on March 7, 2008 as DOI: 10.1124/mol.107.042085
This article has not been copyedited and formatted. The final version may differ from this version.

Figure 7. Blocking kinetics. **(A)** The apparent rate of blocking as a function of cisapride concentration. Curves represent fits with equation 9 (see Methods). The intercepts of the y-axis represents the values of k_{off}. The k_{off} values (/s) for the mutants were as follows: 0.10 ± 0.13 for WT, 0.01 ± 0.15 for td[wt : wt], 0.01 ± 0.08 for td[wt : F656A], 0.03 ± 0.00 for td[wt : Y652AF656A], 0.32 ± 0.16 for td[wt : Y652A] and 3.1 ± 0.4 for F656A. The k_3 values (/s) were 0.015 for WT, 0.022 for td[wt : wt], 0.034 for td[wt : F656A], 0.017 for td[wt : Y652AF656A], 0.017 for td[wt : Y652A] and 0.012 for F656A.The symbols for channel species are shown in A. **(B)** K_f values (μmol/L) obtained from fitting the data shown in A. The fit parameters roughly reproduced the K_i values obtained from the concentration dependence of the steady-state block. Nearly linear relationships suggest that experiments were performed in the concentration range below the K_f value for each channel species.

Figure 8. Energetics and orientation of cisapride binding. **(A)** The thermodynamic double-mutant cycle analysis. Cartoons for mutant channels are presented without the linker to show differences in special arrangements of residues between mutant channels. Orange arrows represent mutations from Y_{652} to A and blue ones for $F_{656} \rightarrow$ A. There are two pathways to get double mutants: Firstly, $Y_{652} \rightarrow$ A (the upper orange arrow), then $F_{656} \rightarrow$ A (the right blue arrow). Another route is $F_{656} \rightarrow$

Molecular Pharmacology Fast Forward. Published on March 7, 2008 as DOI: 10.1124/mol.107.042085
This article has not been copyedited and formatted. The final version may differ from this version.

A (the left blue arrow) first and $Y_{652} \rightarrow$ A (the lower orange arrow) later. The upper panel shows the cycle to td[wt : Y652AF656A] and the lower to td[Y652A : F656A]. Numerical values indicate ΔGs (see Methods). The parallelogram indicates the level of the binding free energy for td[wt : wt], from which up and down arrows were drawn for ΔGs. The changes in the binding energy from td[wt : wt] to td[wt : Y652AF656A] were evaluated by the sums of ΔGs through either of the pathways ($\Delta G_{\text{singleM1-WT}} + \Delta G_{\text{doubleM-singleM1}} = \Delta G_{\text{singleM2-WT}} + \Delta G_{\text{doubleM-singleM2}}$). If two residues contribute to the binding independently, ΔG of a mutation at one site should not depend on whether another site is intact or mutated ($\Delta G_{\text{singleM1-WT}} = \Delta G_{\text{doubleM-singleM2}}$). This is seen in the mutations from td[wt : wt] to td[wt : Y652A] (ΔG = 3.0 kJ/mol) and from td[wt : F656A] to td[wt : Y652AF656A] (ΔG = 2.7 kJ/mol) and the $\Delta\Delta G_{\text{int}}$ value was 0.3 kJ/mol. For the double-mutant cycle in the lower panel, the $\Delta\Delta G_{\text{int}}$ value was -3.1 kJ/mol. As seen from the double-mutants for both cycles, the coupling energy represents interactions between Y_{652} and F_{656} in the same subunit and in the adjacent subunits. Significant interaction suggests that Y_{652} and F_{656} from different subunits located in proximity. **(B)** Chemical structure of cisapride and a hypothetical binding topology. Red lines indicate positive interaction while the blue dotted line indicates negative contributions. In this scheme bindings are restricted to the adjacent two subunits.

Molecular Pharmacology Fast Forward. Published on March 7, 2008 as DOI: 10.1124/mol.107.042085
This article has not been copyedited and formatted. The final version may differ from this version.

Figure 9. A hypothetical binding model for cisapride. A scheme for the longitudinal section of the HERG pore from the cytoplasmic entryway to the central cavity is shown. B_1 and B_2 represent the low- and high-affinity binding states. Orange arrows indicate voltage-dependent rearrangements of Y_{652} residues.

Molecular Pharmacology Fast Forward. Published on March 7, 2008 as DOI: 10.1124/mol.107.042085
This article has not been copyedited and formatted. The final version may differ from this version.

Tables

Table 1. Mutant constructs of HERG channels.

HERG Channel	Mutations	
Homo-tetramer		
WT	**Wild type**	
Y652A	**Y652A**	
F656A	**F656A**	
Tandem dimer	***N-terminal side***	***C-terminal side***
td[wt : wt]	**Wild type**	**Wild type**
td[wt : Y652A]	**Wild type**	**Y652A**
td[wt : F656A]	**Wild type**	**F656A**
td[wt : Y652AF656A]	**Wild type**	**Y652A + F656A**
td[Y652A : F656A]	**Y652A**	**F656A**

In this study the mutants were named in the conventional manner for homo-tetrameric channels (such as F656A). For tandem dimers single or double mutations were expressed in a square bracket introduced into the N- and C-terminal subunits separated by a colon for the linker.

Molecular Pharmacology Fast Forward. Published on March 7, 2008 as DOI: 10.1124/mol.107.042085
This article has not been copyedited and formatted. The final version may differ from this version.

Table 2. Gating properties of HERG channels

	Activation		Inactivation		
HERG Channels	**$V_{1/2}$ (mV)**	**Slope (mV)**	**$V_{1/2}$ (mV)**	**Slope (mV)**	**N**
WT	**-21.0 ± 0.7**	**7.2 ± 0.2**	**-61.6 ± 4.5**	**-26.7 ± 1.1**	**8**
td[wt : wt]	**-22.2 ± 0.8**	**7.0 ± 0.2**	**-61.4 ± 3.5**	**-26.2 ± 0.9**	**9**
td[wt : F656A]	**-25.1 ± 0.8**	**7.3 ± 0.1**	**-60.2 ± 4.0**	**-30.2 ± 1.0**	**10**
td[wt : Y652A]	**-24.3 ± 1.1**	**7.6 ± 0.1**	**-51.4 ± 4.6**	**-32.1 ± 1.1**	**10**
td[wt : Y652AF656A]	**-24.2 ± 0.4**	**7.7 ± 0.2**	**-56.7 ± 4.9**	**-28.3 ± 1.9**	**9**
td[Y652A : F656A]	**-25.7 ± 0.7**	**7.5 ± 0.2**	**-57.0 ± 4.9**	**-36.6 ± 1.2**	**10**
F656A	**-27.3 ± 0.7**	**6.7 ± 0.1**	**-87.1 ± 4.6**	**-41.7 ± 3.0**	**12**
Y652A	**-22.4 ± 0.6**	**7.6 ± 0.1**	**-50.0 ± 3.7**	**-35.5 ± 1.1**	**10**

The half activation and inactivation voltages ($V_{1/2}$) and their slopes are shown.

N represents the number of observations.

Molecular Pharmacology Fast Forward. Published on March 7, 2008 as DOI: 10.1124/mol.107.042085
This article has not been copyedited and formatted. The final version may differ from this version.

Table 3. Blocking parameters of cisapride to HERG channels at +20 mV.

HERG Channel	K_i (μmol/L)	Hill coefficient	N
WT	0.20 ± 0.02	0.96 ± 0.05	4
td[wt : wt]	0.25 ± 0.01	1.36 ± 0.07	4
td[wt : F656A]	0.17 ± 0.01	1.04 ± 0.05	5
td[wt : Y652A]	0.85 ± 0.06	1.15 ± 0.09	5
td[wt : Y652AF656A]	0.50 ± 0.05	1.10 ± 0.05	5
td[Y652A : F656A]	2.05 ± 0.04	1.19 ± 0.01	5
F656A	3.63 ± 0.44	0.99 ± 0.09	6
Y652A	9.15 ± 0.67	1.23 ± 0.11	5

These K_i values represent drug binding at depolarized potential of +20 mV, since unblocking was slow and could not be detected at the time of peak-current measurements for most of the channel species except for F656A. The K_i value for F656A at +20 mV was obtained by correcting for the unblocking component at the tail potential (see Supplemental data). N represents the number of observations.

Figure 1

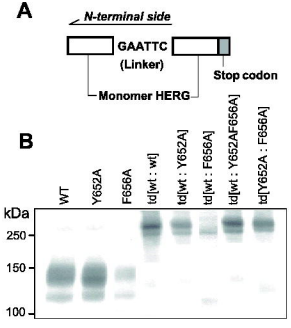
A
N-terminal side
GAATTC
(Linker)
Stop codon
Monomer HERG
B
WT
Y652A
F656A
td[wt : wt]
td[wt : Y652A]
td[wt : F656A]
td[wt : Y652AF656A]
td[Y652A : F656A]
kDa
250
150
100

Figure 2

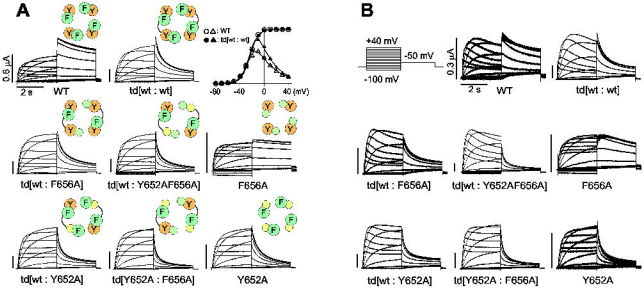
A
B
0.6 μA
2 s
WT
td[wt : wt]
○△: WT
●▲: td[wt : wt]
-80
-40
0
40 (mV)
td[wt : F656A]
td[wt : Y652AF656A]
F656A
td[wt : Y652A]
td[Y652A : F656A]
Y652A
+40 mV
-50 mV
-100 mV
0.3 μA
2 s
WT
td[wt : wt]
td[wt : F656A]
td[wt : Y652AF656A]
F656A
td[wt : Y652A]
td[Y652A : F656A]
Y652A

Figure 3

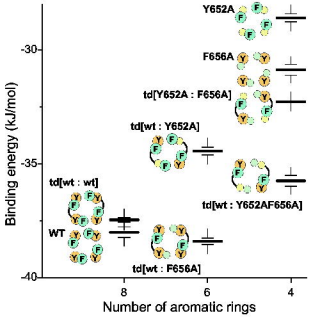
Y652A
F656A
td[Y652A : F656A]
td[wt : Y652A]
td[wt : wt]
td[wt : Y652AF656A]
WT
td[wt : F656A]
-30
-35
-40
8
6
4
Binding energy (kJ/mol)
Number of aromatic rings

Figure 4

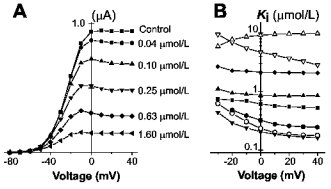
A
(μA)
1.0
Control
0.04 μmol/L
0.10 μmol/L
0.25 μmol/L
0.63 μmol/L
1.60 μmol/L
-80
-40
0
40
Voltage (mV)
B
Ki (μmol/L)
10
1
0.1
-20
0
20
40
Voltage (mV)

Figure 5

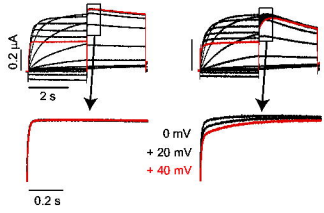

Figure 6

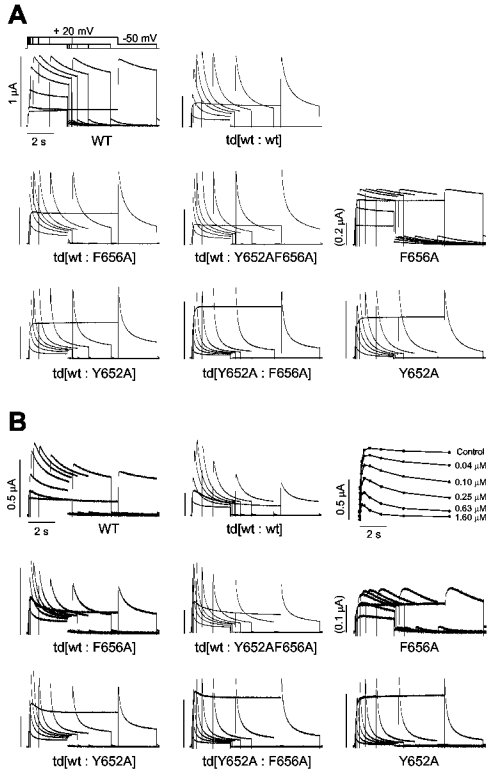
A
+ 20 mV
-50 mV
1 µA
2 s
WT
td[wt : wt]
td[wt : F656A]
td[wt : Y652AF656A]
(0.2 µA)
F656A
td[wt : Y652A]
td[Y652A : F656A]
Y652A
B
0.5 µA
2 s
WT
td[wt : wt]
Control
0.04 µM
0.10 µM
0.25 µM
0.63 µM
1.60 µM
0.5 µA
2 s
td[wt : F656A]
td[wt : Y652AF656A]
(0.1 µA)
F656A
td[wt : Y652A]
td[Y652A : F656A]
Y652A

Figure 7

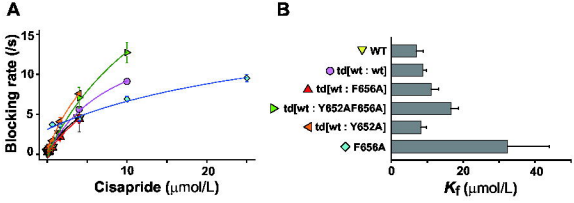
A
Blocking rate (/s)
15
10
5
0
10
20
Cisapride (μmol/L)
B
WT
td[wt : wt]
td[wt : F656A]
td[wt : Y652AF656A]
td[wt : Y652A]
F656A
0
20
40
K_f (μmol/L)

Figure 8

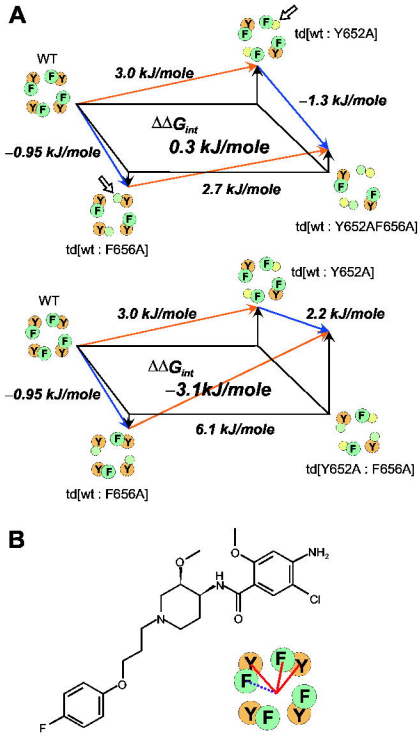
A
td[wt : Y652A]
WT
3.0 kJ/mole
−1.3 kJ/mole
ΔΔG_int
0.3 kJ/mole
−0.95 kJ/mole
2.7 kJ/mole
td[wt : Y652AF656A]
td[wt : F656A]
td[wt : Y652A]
WT
3.0 kJ/mole
2.2 kJ/mole
ΔΔG_int
−3.1kJ/mole
−0.95 kJ/mole
6.1 kJ/mole
td[Y652A : F656A]
td[wt : F656A]
B
NH2
Cl
O
H
N
F

Figure 9

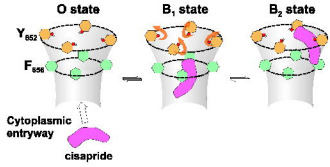
O state
B1 state
B2 state
Y652
F656
Cytoplasmic entryway
cisapride

Supplemental data

Basic gating properties of the mutants

Voltage-dependent gating

To characterize the activation gate for mutant channels, the peak amplitudes for the tail current at -50 mV were plotted as a function of the preceding activation voltages (the tail *I-V*; Fig. S1, sigmoidal curves). For the inactivation gate the current amplitudes at the end of the 3 s depolarization pulses (isochronal *I-V* curves) were drawn, which were superimposed on the tail *I-V* curves for each channel species (Fig. S1). The isochronal *I-V* curves show a typical bell shape, indicating the characteristic inactivation of HERG channel.

The activation gating was slightly shifted by mutations. Among them the effect of F656A was prominent. The shifts of the activation curve were additive as the numbers of F_{656} were decreased, suggesting the stabilizing effects of F_{656} residues for the closed gate structure. The effects of Y_{652}-deletion on the activation gating were weaker. In fact, total loss of Y_{652} did not shift $V_{1/2}$.

In contrast to the activation gating, the effects of the mutation on the inactivation were more prominent. Most of the mutants destabilized the inactivation, indicating contributions of these residues to the inactivation gating. It is noted that the shifts of $V_{1/2}^{inac}$ seemed to be negatively correlated with those for the activation. The opposite directions of the shifts of $V_{1/2}$ for the activation and inactivation made the variations of relative amplitude for the tail and isochronal *I-V*s among mutants prominent. Compared to these shifts, the slope factors, for both activation and inactivation, were not changed significantly by mutations.

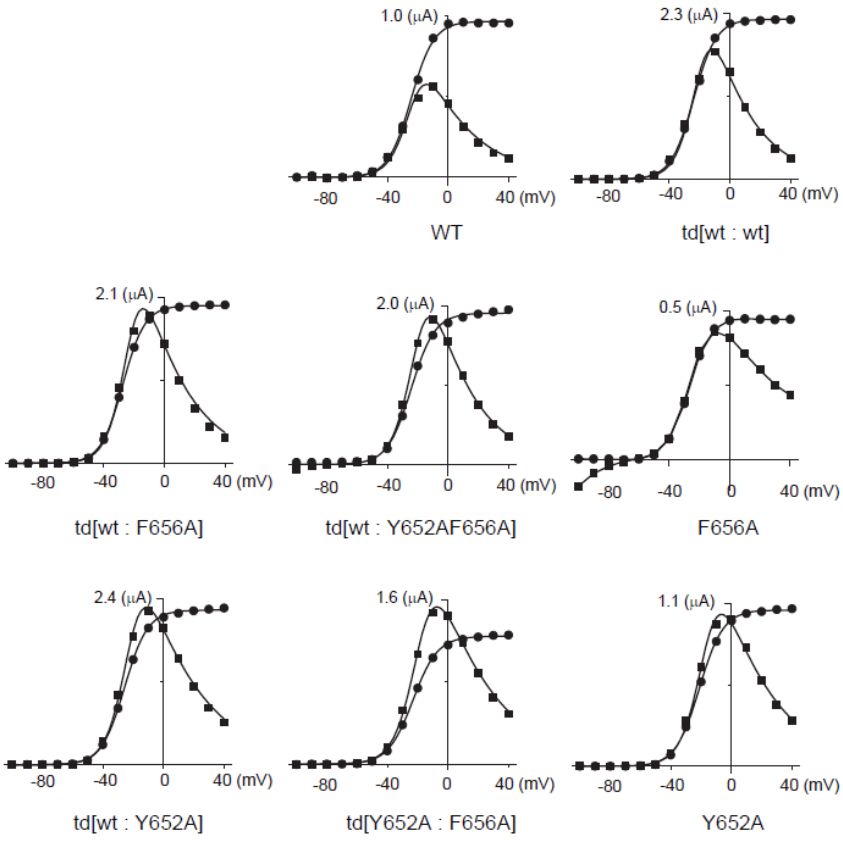

Figure S1. Voltage-dependent gating of HERG channels. Tail I-V curves and the isochronal I-V curves at the end of the depolarization pulses. Note that for F656A the inward currents were recorded at negative potentials.

Voltage-dependent blocking of mutant channels

As has been shown in the main text, the voltage-dependent blocking was examined using the tail

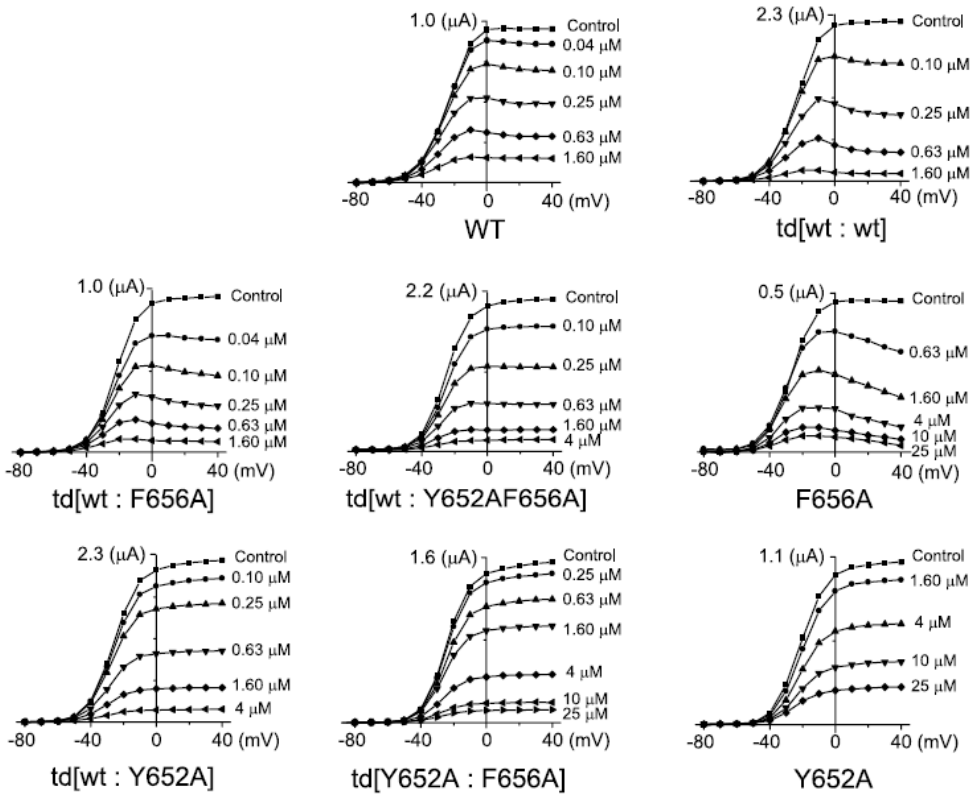

Figure S2. Voltage-dependent blocking of HERG channels by cisapride. The tail *I-V* curves at various concentrations of cisapride are shown for WT and mutants.

I-V curves for different concentration of cisapride. Here the tial *I-V* curves for mutant channels are shown (Figure S2). K_i values were obtained from the concentration-dependence of peak amplitudes for the tail current. The K_i values for different membrane potentials were shown in Figure 4B.

Blocking kinetics

Blocking kinetics was evaluated by two different methods: Unblocking kinetics at repolarized potential and slow blocking kinetics from the envelope analysis. Both use the tail current to minimize possible contamination of the endogenous currents.

Unblocking for F656A

In F656A, release of cisapride from the blocked channel was observed at the time of peak for tail current. This unblocking process appeared as a novel kinetic component with the time range faster than deactivation and slower than recovery from inactivation. The time courses of the tail currents for F656A in the presence of cisapride were fitted by a triple-exponential function:

$$I = A_{de-Inact} Exp[-t/\tau_{de-Inact}] + A_{unblock} Exp[-t/\tau_{unblock}] + A_{de-act} Exp[-t/\tau_{de-act}] + C \qquad \text{Eq. S1}$$

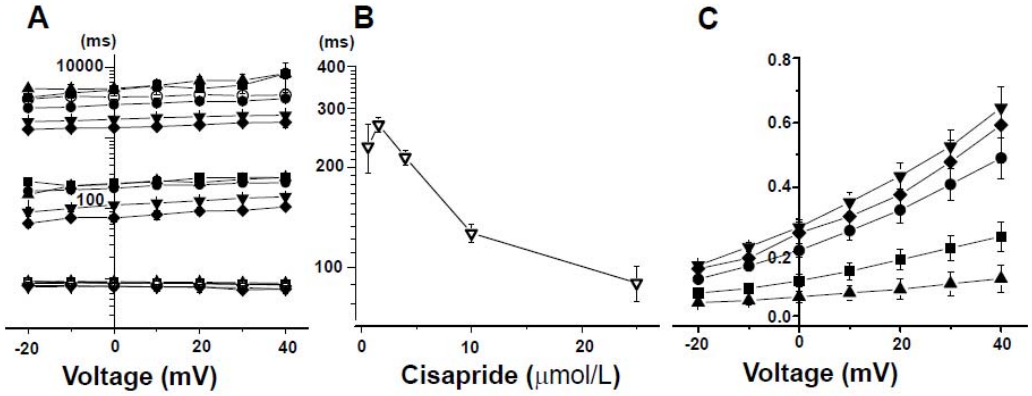

Figure S3. Unblocking kinetics for F656A. (A)Three time constants for the tail currents at different pre-potentials and at different cisapride concentrations. (B)The intermediate time constant at different cisapride concentrations. (C) Fractional amplitudes for the unblocking (intermediate) component. Same symbols are used in the panels A and C, and are indicating cisapride concentrations (μmol/L); ○: 0 (control), ▲: 0.63, ■: 1.6, ●: 4, ▼: 10, ♦: 25 μmol/L.

in which the subscripts represent de-inactivation, unblocking and de-activation, respectively. *C* represents the time-independent component of current.

The time constants were plotted as a function of pre-potentials (Figure S3A). In the absence of cisapride, only fast and slow components were detected (open symbols). Therefore, the intermediate component representes the unblocking process. The three time constants were independent of the pre-potentials, suggesting the fit of the data to be reliable. In Figure S3A the time constants at different cisapride concentration are superimposed. The fast component with the time constant of ~10 ms represents the recovery from the inactivation and is not affected by cisapride. The slow component represents the deactivation and the time constants became smaller at high cisapride concentrations. The time constants for unblocking are plotted as a function of cisapride concentration in Figure S3B and the reciprocal values of the time constant (rate constants) were shown in Figure7A.

Fractional amplitudes of the unblocking component (= $A_{unblock}$ / [$A_{de\text{-}inact}$ + $A_{unblock}$ + $A_{de\text{-}act}$]) at different membrane potentials are shown in Figure S3C. At low concentration of cisapride, the voltage-dependence of unblocking is clearly seen: More fractions of channels showed unblocking at the tail potential when the preceding depolarization potentials were more positive. At high concentration of cisapride, only a fraction of channels showed unblocking.

Voltage-dependent blocking of F656A corrected for unblocking

Since F656A showed fast unblocking at repolarized potentials, current amplitudes at the peak of the tail current do not reflect steady-state blocking at the preceding depolarization potentials. Without correction for unblocking components, the affinity and its voltage-dependence will be underestimated. The amounts of unblocking at the peak of tail currents were estimated from the kinetic parameters obtained from fitting with triple-exponential function (the previous section). The amplitude of the intermediate component of the exponential function corresponds to the unblocking component ($A_{unblock}$), which was subtracted from those of the deactivating component

($A_{de\text{-}act}$). Corrected current amplitudes were used for K_i values and from their voltage-dependence the gating charge (slope factor) was evaluated (Figure 4B legend).

Blocking rates

In this study a simple blocking model was proposed from experimental data for voltage-dependent blocking and blocking kinetics. From the voltage-dependence of the blocking the successive binding model was suggested.

$$O \underset{k_2}{\overset{[B]k_1}{\Leftrightarrow}} B_1 \underset{k_4}{\overset{k_3}{\leftrightarrow}} B_2$$

in which voltage dependence occurs after drug binding rather than upon binding.

If the binding and unbinding kinetics are slow relative to the subsequent transition between B_1 and B_2, the apparent rate constant of blocking show shallow and non-linear dependence on cisapride concentration. Nearly linear relationships observed for most of the channels (Figure 7A) suggest that the binding process is fast. If the initial binding reaction is much faster than the subsequent reaction, the transition between O and B_1 may be approximated as being in equilibrium. Then the probability of B_1 state can be expressed as:

$$P_{B_1} = \frac{[B]k_1}{[B]k_1 + k_2}$$

The rate of blocking becomes

$$blocking\_rate = \frac{[B]k_1}{[B]k_1 + k_2}k_3 + k_4 = \frac{[B]k_3}{[B] + k_2/k_1} + k_4 = \frac{[B]k_3}{[B] + K_f} + k_{off} \qquad \text{Eq. S2}$$

K_f (= k_2/k_1) is the dissociation constant for the initial binding site.

When the concentration of blocker is low compared to K_f, this equation is reduced to the following equation:

$$blocking\_rate = [B]\frac{k_3}{K_f} + k_{off} \qquad \text{Eq. S3}$$

This equation gives linear concentration dependence. The Y-axis intercept gives the off-rate (k_{off}), or k_4 value.

When the blocker concentration becomes close to K_f, non-linearity becomes apparent. Three kinetic parameters were obtained by fitting the equation S2 (Eq. 1 in the main text) to the data (Figure 7A and legends). The K_f, and k_{off} values were listed in the figure legend.